THE ASTROPHYSICAL JOURNAL, 461:288–297, 1996 April 10

A BUTTERFLY IN THE MAKING: REVEALING THE NEAR-INFRARED STRUCTURE OF HUBBLE 12

JOSEPH L. HORA
Institute for Astronomy, 2680 Woodlawn Drive, Honolulu, HI 96822

AND

WILLIAM B. LATTER
NASA/Ames Research Center, MS 245-3, Moffett Field, CA 94035
Received 1995 June 29; accepted 1995 October 13

ABSTRACT

We present deep narrowband near-IR images and moderate resolution spectra of the young planetary nebula Hubble 12. These data are the first to show clearly the complex structure for this important planetary nebula. Images were obtained at $\lambda = 2.12$, 2.16, and 2.26 μm. The $\lambda = 2.12$ μm image reveals the bipolar nature of the nebula, as well as complex structure near the central star in the equatorial region. The images show an elliptical region of emission, which may indicate a ring or a cylindrical source structure. This structure is possibly related to the mechanism that is producing the bipolar flow. The spectra show the nature of several distinct components. The central object is dominated by recombination lines of H I and He I. The core is not a significant source of molecular hydrogen emission. The east position in the equatorial region is rich in lines of ultraviolet–excited fluorescent H_2. A spectrum of part of the central region shows strong [Fe II] emission, which might indicate the presence of shocks.

Subject headings: infrared: ISM: continuum — infrared: ISM: lines and bands — molecular processes — planetary nebulae: individual (Hubble 12)

1. INTRODUCTION

The planetary nebula (PN) Hubble 12 (Hb 12; PN G111.8−02.8) has been notable primarily because it represents one of the clearest cases known of fluorescent molecular hydrogen emission, first determined by Dinerstein et al. (1988) and recently confirmed by Ramsay et al. (1993). The observed H_2 line ratios were found to closely match those calculated by Black & van Dishoeck (1987) for the case of pure fluorescent emission. Objects that exhibit pure fluorescent spectra have proven to be rare, since in regions with strong UV fields and densities $n \gtrsim 10^4$ cm^{-3}, the line ratios are driven to values that are characteristic of "collisional" fluorescent emission (Sternberg & Dalgarno 1989). Shocks are common in PNs, and in most PNs observed to date in which H_2 emission has been detected the H_2 appears to be purely shock-excited or has a significant shock-excited contribution (see, e.g., Beckwith, Persson, & Gatley 1978; Storey 1984; Latter et al. 1993; Aspin et al. 1993; Graham et al. 1993; Kastner et al. 1994; Hora & Latter 1994).

Radio continuum images taken at the VLA have shown Hb 12 to be a bipolar nebula, aligned roughly north–south (Bignell 1983). However, these images showed only parts of the faint bipolar lobes, and no detail of the central region was resolved. Miranda & Solf (1989) obtained long-slit spectroscopy and confirmed the bipolar nature of the source. Their observations showed the nebula to be oriented such that the north lobe is receding and the south lobe approaching. In the course of their spectral observations, Dinerstein et al. (1988) mapped the central region and found the 2.12 μm emission to be distributed in a "doughnut-like" shell with inner and outer dimensions of $r = 4''$ and $8''$. Such structures in the equatorial regions of bipolar PNs might be important in understanding the process of the onset of asymmetry and the shaping of PNs by stellar winds. We have, therefore, obtained deep H_2 images and spectra of Hb 12 to further probe the nature of this important and unusual nebula.

2. OBSERVATIONS AND DATA REDUCTION

Near-IR images of Hb 12 were obtained during 1995 January 21–22 UT with the University of Hawaii (UH) Quick Infrared Camera (QUIRC) at the UH 2.2 m telescope on Mauna Kea. This is a new instrument that utilizes a 1024 × 1024 pixel "HAWAII" array (Kozlowski et al. 1994). The telescope was used in the f/10 configuration, giving a pixel size of $0''.18$ pixel^{-1}. The camera currently holds eight filters manufactured by Barr Associates, including their narrowband ($\approx 1\%$) filters at $\lambda = 2.12$ and 2.16 μm, and a 2.26 (2.7%) μm continuum filter. The image presented here was constructed of separate exposures that were individually sky-subtracted and flat-fielded before shifting and averaging. The images are shown in Figures 1 (Plate 7) and 2 (Plate 8). The average FWHM of the point sources in the 2.12 μm image is $0''.71$, and the 1 σ noise levels are 7×10^{-5}, 1.1×10^{-4}, and 5×10^{-5} Jy arcsec^{-2} for the 2.16, 2.26, and 2.12 μm images, respectively. Flux calibration was performed using the standard star HD 3029, which was assumed to have a magnitude of 7.09 in each of the narrowband filters, based on the K-band magnitude of Elias et al. (1982).

Figure 2*b* shows a continuum-subtracted image at 2.12 μm. The subtraction was performed by using the 2.26 μm image, scaled by a factor obtained by comparing the continuum levels at 2.26 and 2.12 μm in the spectrum of the $3''.7$ E position (see below). The 2.26 μm image has higher noise than the original 2.12 μm image, so the continuum-subtracted image is slightly degraded. By scaling the continuum image to the extended emission spectrum, we have not matched the continuum level of the core. Therefore, we have masked the central $\sim 3''$ where the subtraction is invalid. A slight mismatch of the PSF between the two wavelengths is visible in the small artifacts around each of the field stars. Furthermore, there is some contribution to the flux in the 2.26 μm image from some lines of H_2, primarily from the

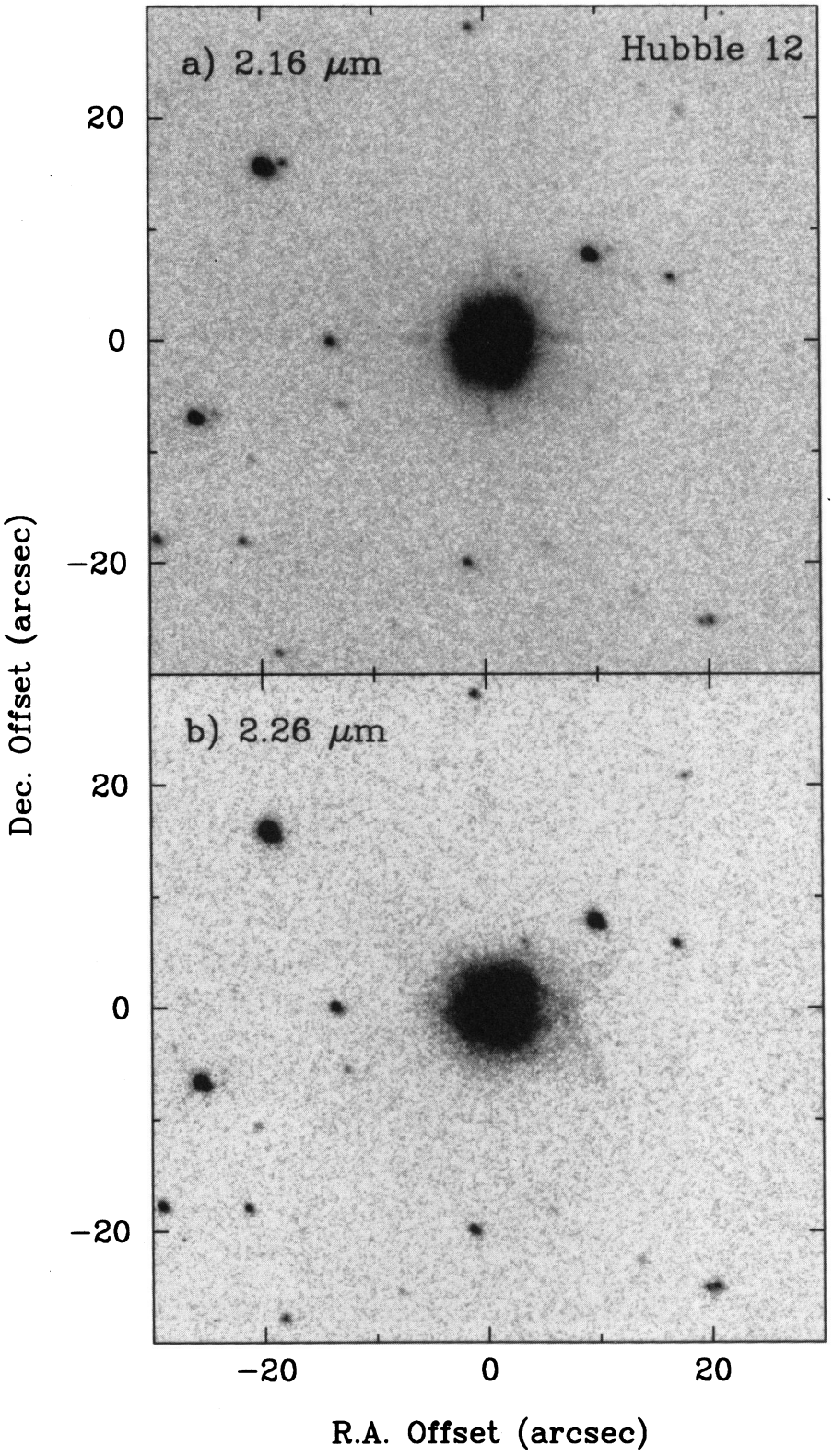

FIG. 1.—Planetary nebula Hubble 12. North is up, and east is to the left in all images. (*a*) Image taken with the Brγ filter at 2.16 μm; (*b*) continuum (2.26 μm filter).

PLATE 8

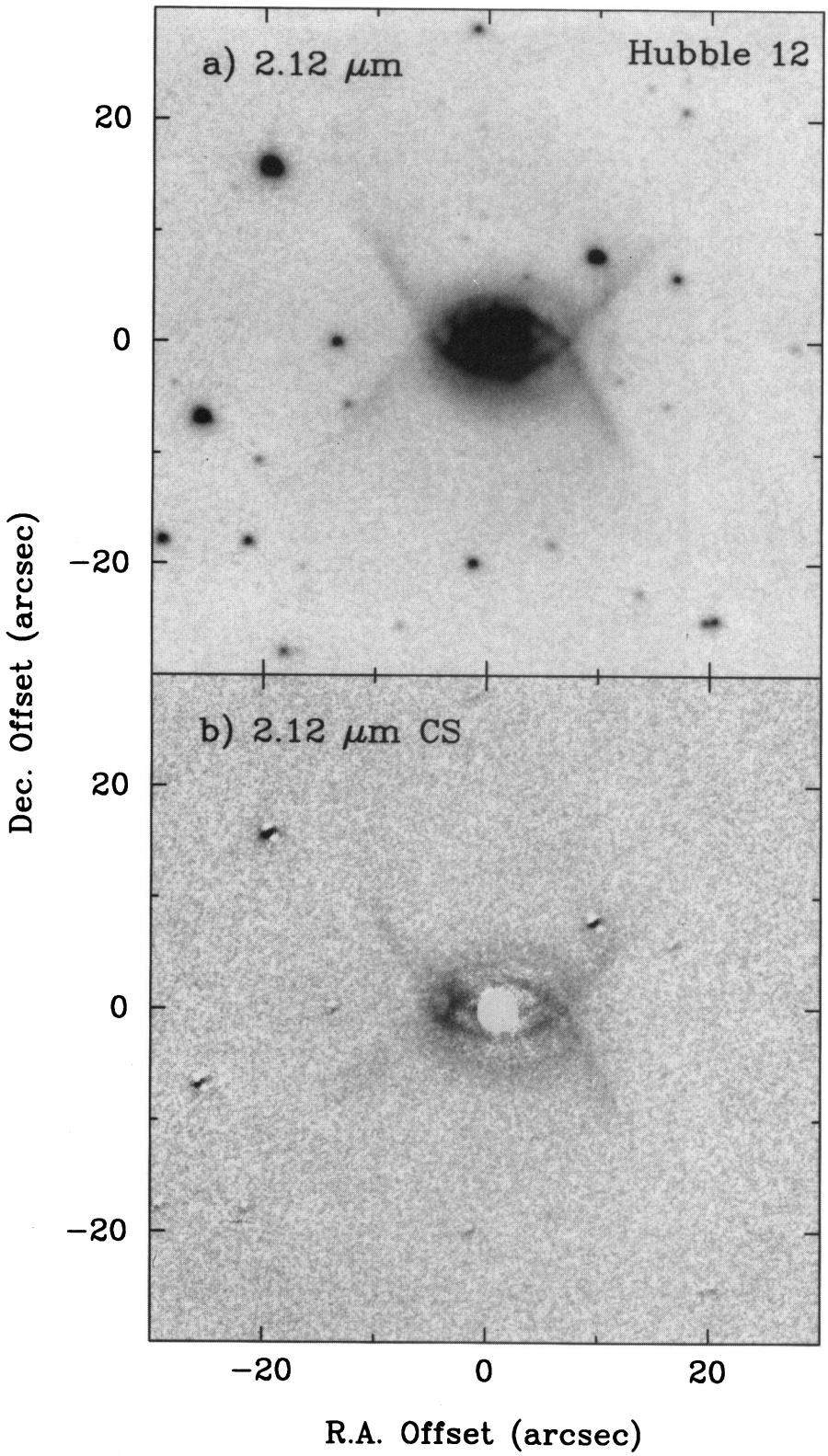

FIG. 2.—Planetary nebula Hubble 12 at 2.12 μm. North is up, and east is to the left in all images. (*a*) 2.12 μm image of Hb 12; (*b*) continuum-subtracted image, obtained by subtracting a scaled 2.26 μm image from the 2.12 μm image in (*a*). The central ~3″ has been masked where the continuum level is not well matched.

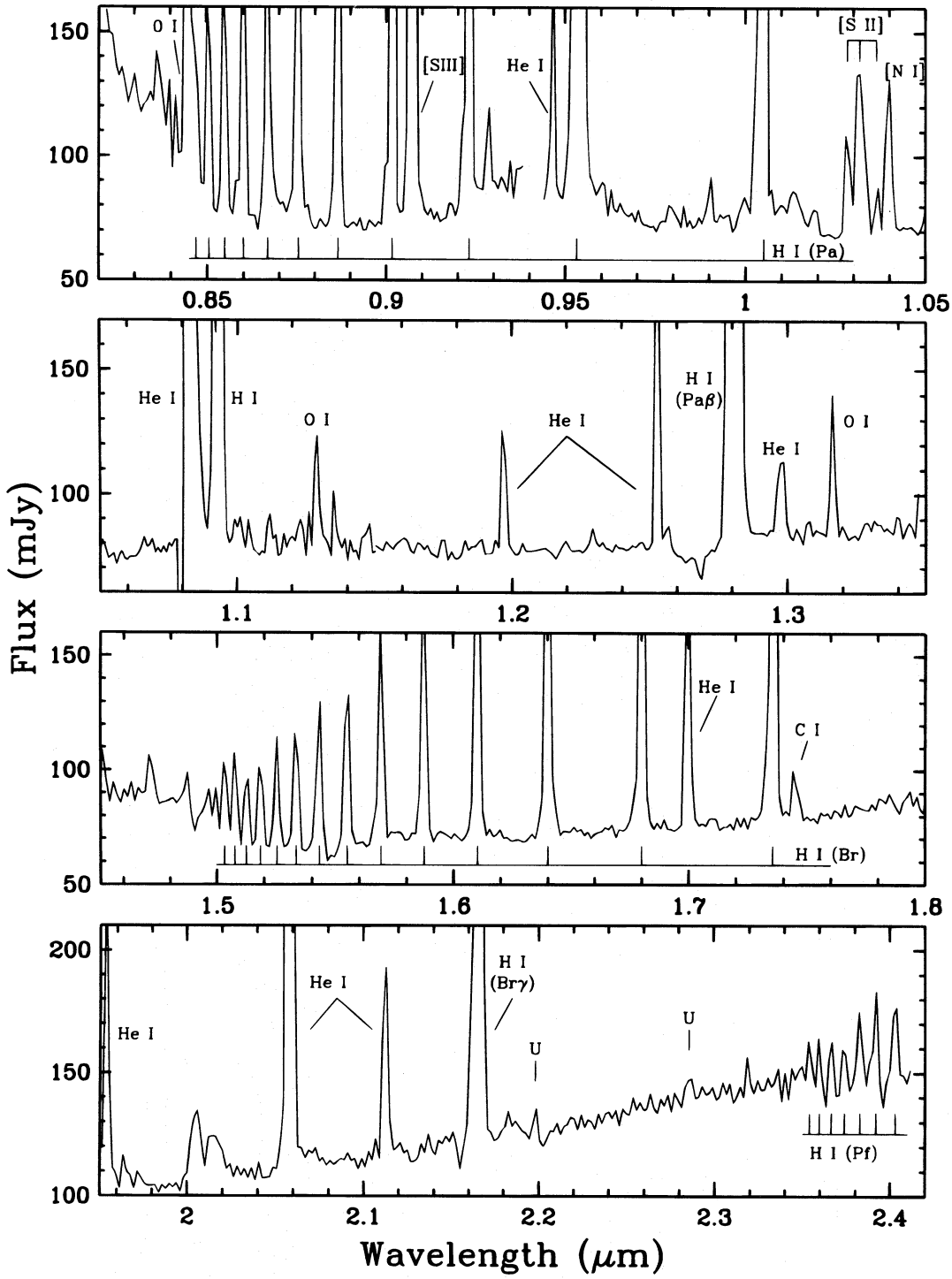

FIG. 3.—Spectra of Hubble 12, at the core position. The wavelength positions of lines of H I, He I, and other strong lines are indicated. Note that the wavelength scales for each of the ranges are slightly different. The apparent emission features between 2.0 and 2.02 μm are due to differences in the atmospheric absorption when the reference star data were taken.

(2, 1) $S(1)$ line at 2.248 μm. This is probably contributing to the extended emission visible in the 2.26 μm image in Figure 1*b*. However, the continuum-subtracted image shows that at 2.12 μm line emission from H_2 dominates and that it is extended in the equatorial region and in the bipolar lobes.

The spectroscopic observations were performed on 1994 September 25 UT on the UH 2.2 m telescope using the near-IR spectrometer KSPEC (Hodapp et al. 1994). The instrument was configured with a 1″.0 × 6″.5 slit, providing a resolving power of $\lambda/\Delta\lambda \sim 700$. Images were taken simultaneously with the spectral integrations using the slit-viewing detector, allowing for accurate placement and guiding. Integrations were done at two slit positions, one centered on the bright nebular core, and the other at a position 3″.7 east, with the long dimension of the slit oriented N-S. The extracted length of the slit was 2″ for the core, 2″.5 for the 3″.7 E region, and 2″ for the 3″.7 E, 2″ S region (see discussion of regions below). Alternating source and sky integrations were taken and differenced to remove sky and telescope background flux. The on-source integration times were 150

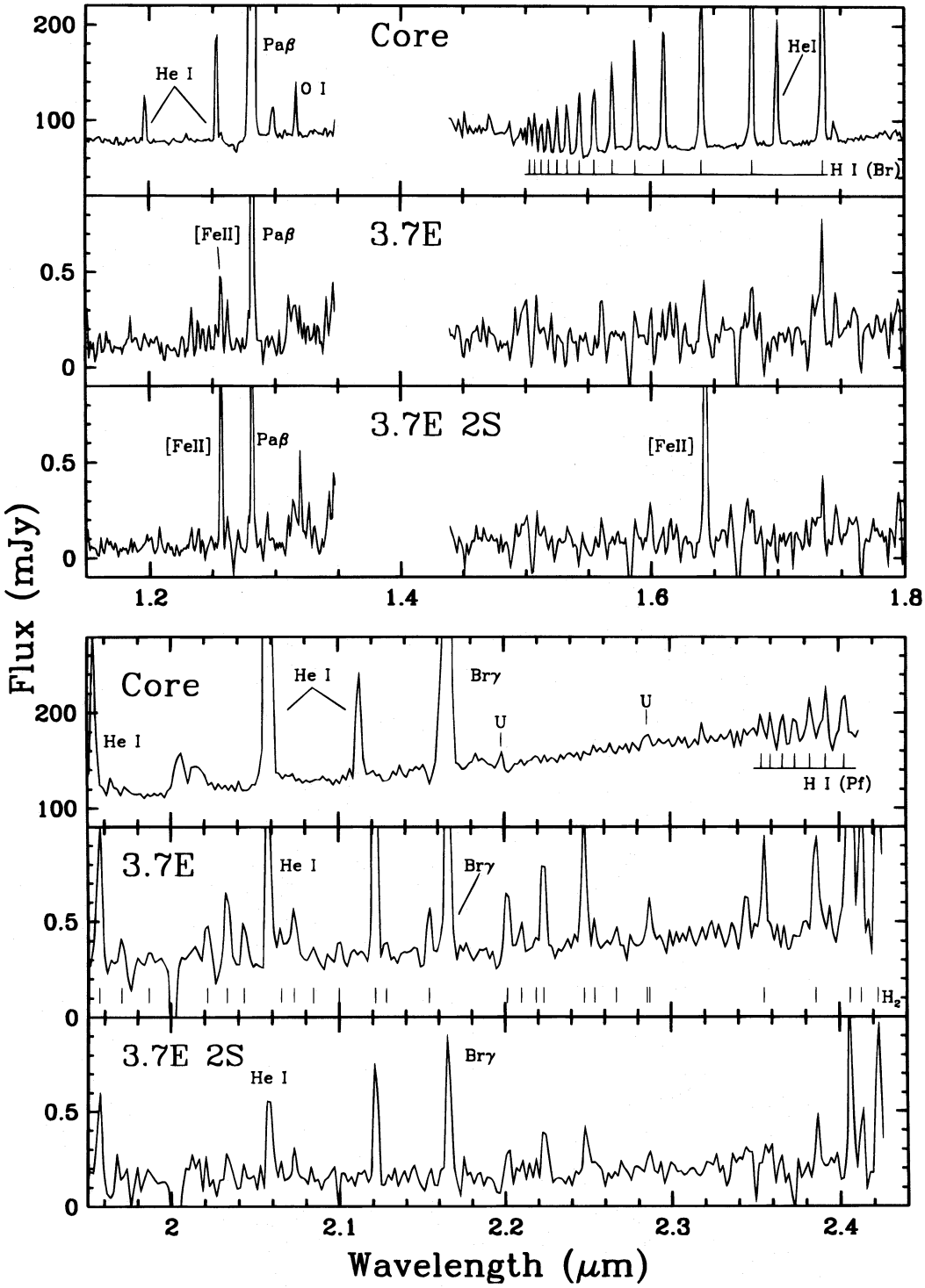

FIG. 4.—Spectra of Hubble 12 at the 3.″7 E, 0″ N and 3.″7 E, 2″ S positions, shown with the core spectrum for comparison. The wavelength positions of lines of H I, He I, H_2, and other strong lines are indicated.

s on the core and 1260 s for the off-core positions. The data were reduced and calibrated as described in Hora & Latter (1994), using the star SAO 35265 for atmospheric correction and HD 44612 as a flux standard. The 0.84–2.43 μm spectrum was extracted for the core, and the 1.15–2.43 μm spectra were extracted for the off-core positions. The spectra of Hb 12 are shown in Figures 3 and 4, and a list of the lines detected is given in Table 1. The absolute calibration is uncertain to 15%–20%, but the measurement of relative line flux and line ratios is much more accurate. The estimated 1 σ noise in the line flux is $\sim 3 \times 10^{-15}$ erg cm^{-2} s^{-1} for the core spectrum and $\sim 1 \times 10^{-16}$ erg cm^{-2} s^{-1} for the off-core positions.

3. RESULTS AND DISCUSSION

The image shown in Figure 2 reveals that the nebula has faint bipolar lobes and an elliptical equatorial region with streamers, along with a compact core. There is a faint halo surrounding the equatorial region that might be associated with it or the bipolar lobes. There is an intersection of features in the equatorial region at the position $\sim 4''$ east of the core where a local maximum of H_2 emission exists. That is

TABLE 1

HUBBLE 12 LINE RATIOS

Wavelength[a] (Å)	Core	Nebula Region Ratios[b] 3″.7 E	3″.7 E, 2″ S	Identification
8448	0.534	...	...	O I
8470	0.126	...	...	Pa17 H I
8505	0.174	...	...	Pa16 H I
8549	0.211	...	...	Pa15 H I
8601	0.234	...	...	Pa14 H I
8668	0.283	...	...	Pa13 H I
8753	0.336	...	...	Pa12 H I
8865	0.416	...	...	Pa11 H I
9017	0.648	...	...	Pa10 H I
9070	5.981	...	...	[S III]
9231	0.851	...	...	Pa9 H I
9285	0.053	...	...	?
9465	0.118	...	...	He I
9532	19.913	...	...	Pa8, [S III]
9903	0.022	...	...	C II?
10029	0.029	...	...	He I?
10051	1.456	...	...	Pa7 H I
10283	0.078	...	...	[S II]
10317	0.158	...	...	[S II]
10364	0.026	...	...	[S II]
10397	0.119	...	...	[N I]
10832	6.284	...	...	He I
10914	0.143	...	...	He I
10936	2.898	...	...	Pa6 H I
11290	0.079	...	...	O I
11354	0.022	...	...	O I?
11510	...	0.372	0.501	H_2 (3, 1) S(5)?
11612	...	0.196	0.267	?
11666	...	0.141	0.327	H_2 (3, 1) S(4)
11687	...	0.088	0.267	H_2 (8, 5) S(0)
11851	...	0.246	0.207	H_2 (3, 1) S(3)
11892	...	0.129	0.200	H_2 (2, 0) S(0)
11986	0.075	...	...	He I
12069	...	0.235	0.373	H_2 (3, 1) S(2)
12143	...	...	0.027	H_2 (8, 5) Q(3)
12213	...	...	0.147	H_2 (11, 7) O(3)
12258	...	0.193	0.087	H_2 (4, 2) S(5)
12294	0.014	...	...	?
12329	...	0.372	0.480	H_2 (3, 1) S(1)
12383	...	0.246	0.507	H_2 (2, 0) Q(1)
12420	...	0.188	...	H_2 (2, 0) Q(2)+(4, 2) S(4)
12469	...	0.193	0.153	H_2 (2, 0) Q(3)
12529	0.160	0.196	0.147	He I
12566	0.015	0.598	3.113	[Fe II]
12618	...	0.317	0.267	H_2 (3, 1) S(0)+(9, 6) S(1) +(4, 2) S(3)
12696	...	0.091	0.367	H_2 (8, 5) O(3)
12740	...	0.011	0.087	H_2 (2, 0) Q(6)
12784	0.268	0.179	0.433	He I
12817	4.348	3.387	3.400	Pa5 (Paβ) H I
12869	...	...	0.180	H_2 (2, 0) Q(7)
12928	...	...	0.600	H_2 (2, 0) O(2)
12977	0.059	...	...	He I
12978	...	...	0.247	H_2 (5, 3) S(6)
13108	...	0.457	0.567	H_2 (5, 3) S(5)+(4, 2) S(1)
13155	...	0.460	0.567	H_2 (9, 6) Q(1)
13162	0.058	...	...	O I
13184	...	0.307	1.393	?
13237	...	...	0.327	H_2 (3, 1) Q(3)
13266	...	...	0.753	H_2 (5, 3) S(4)
14925	...	0.272	0.380	H_2 (5, 3) Q(1)
14960	0.019	...	...	Br25 H I
14976	...	0.290	0.420	H_2 (5, 3) Q(2)
14994	0.017	...	...	C I
15010	...	0.372	0.540	H_2 (6, 4) S(1)
15033	0.036	...	...	Br 23 H I
15076	0.037	...	...	Br 22 H I
15090	...	0.340	0.480	H_2 (4, 2) O(3)
15126	0.036	...	...	Br21 H I
15147	...	0.193	0.373	H_2 (5, 3) Q(4)
15184	0.039	...	...	Br20 H I
15205	...	0.196	0.180	H_2 (3, 1) O(5)
15254	0.044	...	...	Br19 H I

TABLE 1—*Continued*

Wavelength[a] (Å)	Core	Nebula Region Ratios[b] 3.″7 E	3.″7 E, 2″ S	Identification
15335	0.058	...	...	Br18 H I
15432	0.068	...	...	Br17 H I
15549	0.082	...	...	Br16 H I
15567	...	0.085	0.227	?
15610	...	0.381	0.513	H_2 (7, 5) $S(3)+(5, 3)$ $Q(7)$
15693	0.093	...	...	Br15 H I
15875	0.116	...	...	Br14 H I
15877	...	0.229	0.440	H_2 (7, 5) $S(2)$
15920	...	0.094	...	?
16005	...	0.232	0.720	H_2 (6, 4) $Q(1)$
16095	...	0.188	0.300	?
16102	0.149	...	...	Br13 H I
16149	...	0.282	0.480	H_2 (6, 4) $Q(3)$
16204	...	0.229	...	?
16269	...	0.138	...	H_2 (6, 4) $Q(4)$
16401	0.179	...	...	Br12 H I
16432	...	0.469	3.873	[Fe II]
16750	...	0.217	1.013	H_2 (6, 4) $O(2)$
16801	0.211	...	...	Br11 H I
16801	...	0.436	0.773	Fe I?
16867	...	0.243	...	H_2 (4, 2) $O(6)$?
16997	0.113	...	...	He I
17280	...	0.222	0.327	H_2 (7, 5) $Q(1)$
17317	...	0.220	0.320	H_2 (6, 4) $O(3)$
17352	...	0.484	0.567	H_2 (7, 5) $Q(2)$
17356	0.291	...	...	Br10 H I
17446	0.016	...	...	C I
17459	...	0.249	0.480	H_2 (7, 5) $Q(3)$
19541	0.092	...	...	He I
19570	...	0.657	1.253	H_2 (1, 0) $S(3)$
19703	...	0.164	...	H_2 (8, 6) $O(2)$
19868	...	0.097	...	H_2 (9, 7) $S(0)$
20217	...	0.285	0.180	H_2 (7, 5) $O(5)$
20334	...	0.378	0.327	H_2 (1, 0) $S(2)$
20435	...	0.182	0.200	H_2 (8, 6) $O(3)$
20580	0.936	0.815	0.946	He I
20656	...	0.167	0.213	H_2 (3, 2) $S(5)$
20732	...	0.258	0.580	H_2 (2, 1) $S(3)$
20847	...	0.076	0.173	H_2 (9, 7) $Q(2)$
21001	...	0.091	...	H_2 (9, 7) $Q(3)$
21124	0.063	...	...	He I
21218	...	1.000	1.000	H_2 (1, 0) $S(1)$
21284	...	0.137	...	H_2 (3, 2) $S(4)$
21542	...	0.205	...	H_2 (2, 1) $S(2)$
21658	1.000	0.991	1.180	Br7 (Brγ) H I
21982	0.008	...	...	U[c]
22014	...	0.258	0.333	H_2 (3, 2) $S(3)$
22099	...	0.111	0.133	H_2 (8, 6) $O(5)$
22188	...	0.050	0.160	?
22234	...	0.358	0.520	H_2 (1, 0) $S(0)$
22479	...	0.466	0.473	H_2 (2, 1) $S(1)$
22542	...	0.085	0.193	H_2 (9, 7) $O(3)$
22672	...	0.059	...	?
22858	0.006	...	...	U[c]
22872	...	0.135	0.253	H_2 (3, 2) $S(2)$
23448	...	0.147	...	H_2 (4, 3) $S(3)+(9, 7)$ $O(4)$
23541	0.011	...	...	Pf28 H I
23553	...	0.261	...	H_2 (2, 1) $S(0)$
23596	0.010	...	...	Pf27 H I
23665	0.011	...	...	Pf26 H I
23739	0.010	...	...	Pf25 H I
23828	0.014	...	...	Pf24 H I
23861	...	0.390	0.326	H_2 (3, 2) $S(1)$
23920	0.017	...	...	Pf23 H I
24031	0.018	...	...	Pf22 H I
24065	...	1.141	0.993	H_2 (1, 0) $Q(1)$
24130	...	0.452	0.393	H_2 (1, 0) $Q(2)$
24231	...	0.736	0.907	H_2 (1, 0) $Q(3)$

[a] These are the measured wavelengths, with a 1 σ error of $\lesssim 5$ Å. For the cases where the same line was seen in more than one component, the value for the core is listed if detected, otherwise the 3.″7 E position is given.

[b] Fluxes are relative to Brγ (3.14×10^{-12} erg cm^{-2} s^{-1}) for the core, and relative to the 2.12 H_2 line for the 3.″7 E (3.41×10^{-15} erg cm^{-2} s^{-1}) and the 3.″7, 2″ S (1.50×10^{-15} erg cm^{-2} s^{-1}) regions. The ratios in this table have not been corrected for extinction. The estimated 1 σ noise in the line fluxes are $\sim 3 \times 10^{-15}$ erg cm^{-2} s^{-1} for the core position and $\sim 1 \times 10^{-16}$ erg cm^{-2} s^{-1} for the off-core positions.

[c] Unidentified lines observed in several other PNs (see text).

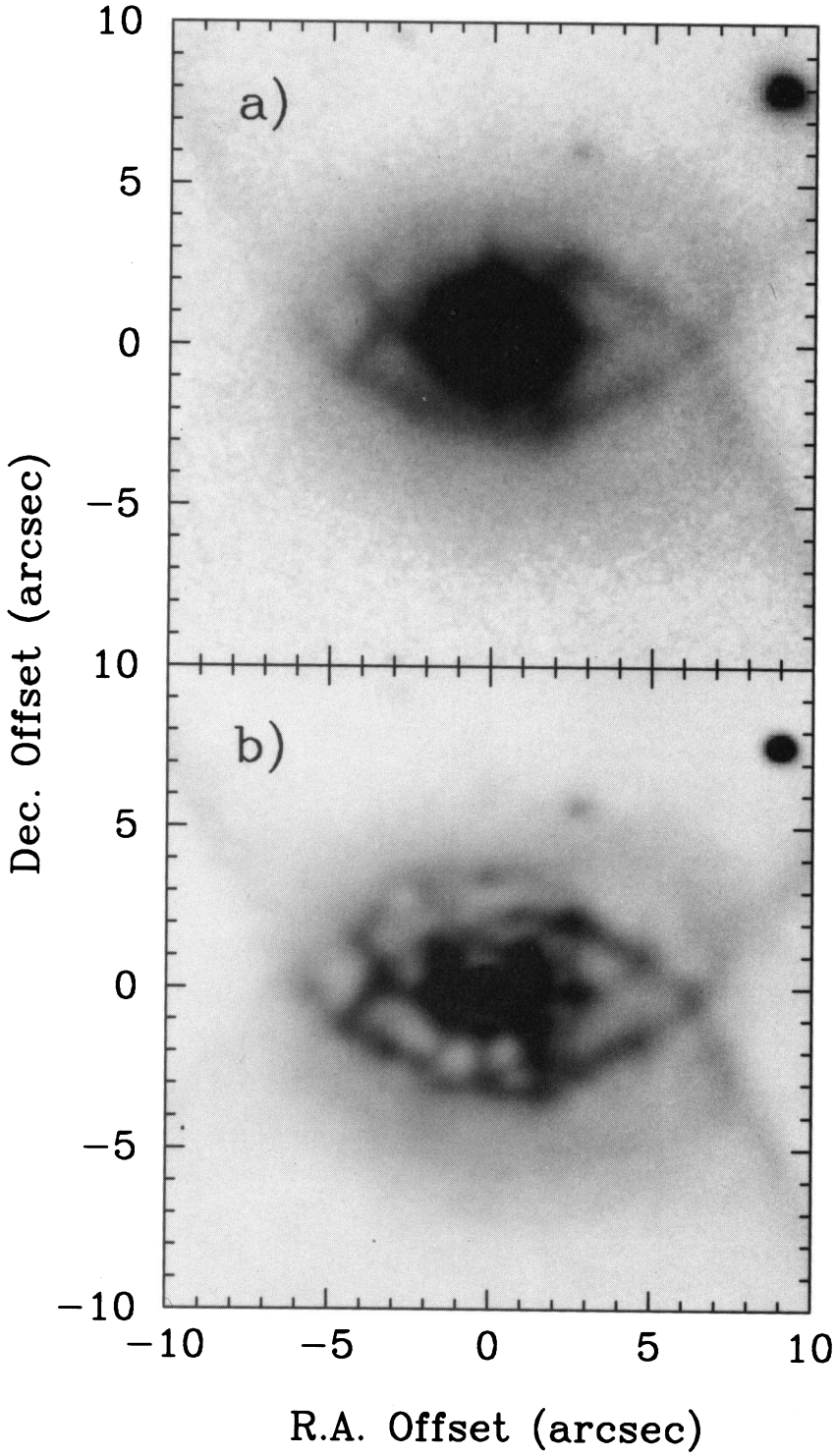

FIG. 5.—The inner 20″ of Hubble 12 at 2.12 μm. (*a*) The original data image (Fig. 2) expanded and rescaled to show the structure of the equatorial region. (*b*) Richardson-Lucy deconvolution of the image in (*a*). The FWHM of point sources has been reduced to ~0.″4 in this image.

the position near where the observations of Dinerstein et al. (1988), Ramsay et al. (1993), and one of the spectra presented here in Figure 4 were centered.

3.1. *The Core*

The core region of the 2.12 μm image (Fig. 2) has a FWHM size of $0''.72 \pm 0''.03$, indistinguishable from the average stellar FWHM of $0''.71$. It is similarly compact at the other observed wavelengths. This is consistent with previous optical and radio observations that showed the nebula to be "stellar" or having a spatial extent of $\lesssim 1''$ (Johnson, Balick, & Thompson 1979; Kohoutek & Martin 1981; Bignell 1983; Miranda & Solf 1989). The spectrum of the core shown in Figure 3 is typical of many PNs, dominated by lines of He I and H I. There is good agreement between the spectrum in Figure 3 and the spectra presented by Rudy et al. (1993) and Kelly & Latter (1995), where the wavelength ranges of the measurements overlap. For example, we measure a Paβ flux of $1.36 \pm 0.20 \times 10^{-11}$ erg cm^{-2} s^{-1}, whereas Rudy et al. obtained 1.13×10^{-11} erg cm^{-2} s^{-1} in a $9''.6 \times 8''.1$ elliptical aperture, and Kelly & Latter found $1.8 \times 10^{-11} \pm 20\%$ erg cm^{-2} s^{-1} in a $6''$ circular aperture. From the O I $\lambda = 1.1287$ to 1.3165 μm line ratio ($=0.3$), Kelly & Latter (1995) argue that the O I emission is UV continuum pumped with no resonant pumping from Lyβ. Our $\lambda = 0.8448$ to 1.3165 μm line ratio ($=9.3$) confirms this result.

No H_2 is detected in the spectrum of the core region, although the brightest H_2 line in the $3''.7$ E spectrum would only be detected at the 3 σ level in this spectrum. It is likely that there is some H_2 emission from the direction of the core, since there will be at least a component due to projection through the equatorial region. However, its relative flux is small compared to other lines and the continuum. For example, the H_2/Brγ line ratio is ~ 1 in the $3''.7$ E position but is $\lesssim 0.03$ in the core. Therefore, the unresolved core itself does not appear to be a significant source of H_2 flux in Hb 12.

Rudy et al. (1993) reviewed estimates of the differential attenuation towards Hb 12. Several estimates, including the Balmer line ratios, indicate an $E(B-V)$ of 0.85. However, they found the Paschen lines showed significant line-to-line departures from Case B ratios, and a fit to their data implied an $E(B-V)$ of 0.45. The Brackett line ratios that we measure have relatively low line-to-line departures from the expected Case B ratios. However, a determination of $E(B-V)$ from our measured values of the Brackett line fluxes gives a value of 0.28 (assuming $T = 10^4$ K and $N_e = 10^6$ cm^{-3}). It is possible that the near-IR line emission is from different regions within the core compared to the optical lines, or that nonstandard extinction effects are present. Luhman & Rieke (1996) also measure anomalous Brackett and Brackett/Pfund line ratios, and suggest that Br10 and Brγ may be optically thick. In that case the $E(B-V)$ values calculated based on expected Case B ratios are not valid.

3.2. *The Equatorial Region and Bipolar Lobes*

3.2.1. *Morphology*

The walls of the bipolar lobes are visible in the H_2 image (Fig. 2) extending roughly N–S with an opening angle of $\sim 70°$, and the axis of the nebula is at a position angle $\sim 2°$ W of N. The distribution of H_2 is similar to the ionized gas as traced by the VLA images. However, if Hb 12 is similar to other PNs such as NGC 7027 (Graham et al. 1993) or M2–9 (Hora & Latter 1994), the H_2 emission is most likely from a region just exterior to the ionized zone (i.e., at a greater radius from the bipolar axis), as determined by the radio continuum emission (Bignell 1983). The lobes are detected out to a total nebular size of $35''$ N–S.

A deconvolution of the central region was performed using the Richardson–Lucy (RL) method implemented in the STSDAS package of IRAF. A star near Hb 12 in the 2.12 μm image was used as the PSF. The result of the deconvolution is shown in Figure 5*b* (Plate 9). Point sources in the deconvolved image were reduced to a FWHM of $\sim 0''.4$. The structure visible in the raw images is significantly enhanced by the deconvolution; the sharp edge of the equatorial region appears incomplete N and E of the core. Brighter spots inside the edge are at the intersection of filamentary structures, rather than in discrete clumps. The deconvolution process does not seem to have created any artificial structure in the extended emission since features visible in the RL image can also be seen in the original. The apparent exception to this is within a radius of $2''$ from the core. This area may have been affected by detector nonlinearities since the core was near saturation in the individual exposures. Artifacts can arise in RL deconvolved images (see, e.g., Linde & Johannesson 1991). We have not performed any independent tests of the validity and possible problems with the RL deconvolution technique. However, none of the conclusions in this paper depend on the accuracy of the RL image in Figure 5*b*.

The filaments and outer edge of the elliptical equatorial region are the locations of UV-excited fluorescent H_2 emission, as seen in Figure 2 and discussed below. Part of the slit overlapped the edge as these data for the east position were taken. We have extracted these data separately and plotted them in Figure 4 (marked as 3.7 E, 2 S). This region appears to have roughly similar H_2 line ratios compared to the $3''.7$ E position. However, strong lines of [Fe II] are seen at $\lambda = 1.644$ and 1.257 μm that are not present or relatively weaker in the core and $3''.7$ E positions. These strong features indicate that a shocked region might be present in the edge. The edge structure might represent a transition between the relatively low-density region inside and higher density outside. The outer edge of the bipolar lobes extend N-S from the equatorial region, indicating some relationship between the equatorial region and the formation of the lobes. The width of the edge emission is not resolved in these images.

There are several possible structures that could explain the observed morphology. One is a ring or torus that encircles the core in a plane perpendicular to the roughly N–S bipolar axis. This was suggested by Dinerstein et al. (1988), who found the H_2 emission to be distributed in an elliptical region around the core. The outer edge of the equatorial zone as shown in Figure 2 is roughly elliptical, with a projected size of $12''.5 \times 6''.9$, and assuming the ring is circular, this implies the ring plane is tipped $\sim 30°$ from the line of sight.

Another possibility is that the observed "ring" structure is significantly distorted from circular, or that the structure is not an equatorial ring but a shell. This is suggested by the fact that the observed structure does not precisely match what one expects from a true ring. In particular, the extreme E and W positions come to a sharp point or cusp rather than being more rounded as one would expect from a torus.

This is illustrated in Figure 6*a*, where a tilted ring has been superimposed on an image of the inner region. Also, the brightness of the emission at the E and W ends is less than or equal to the other parts of the ring. One might expect that these regions would be slightly limb-brightened.

An alternate model of the structure of Hb 12 is a short cylindrical shell. This has been proposed for several other young PNs, such as NGC 7027 (Scott 1973) and BD +30°3639 (Bentley et al. 1984). Recent two-dimensional radiation–gasdynamic simulations by Frank & Mellema (e.g., 1994a) have shown that such structures can be generated by interacting winds with the proper initial conditions. One characteristic of these models is that they reproduce the "eye" appearance as the result of projection of the top and bottom circular edges of the cylinder seen at moderate inclination angles. Figure 6*b* shows the outlines of a cylinder on the central region of the nebula. The inclination angle of the cylinder axis is 50° from the plane of the sky. There is H_2 emission from other parts of the central region that roughly outline the cylindrical shape, but the brightest emission is from the overlapping regions of the ends of the cylinder, looking through what would be the open end. This could be caused by absorption of the emission from the other parts of the cylinder by the material outside of the inner region. The presence of absorbing material is also suggested by the fact that the bipolar lobes that extend to the N and S are brightest at some point around 10″ from the core, not at their closest point. High-resolution spectra of the H_2 emission to determine the velocity structure of the equatorial region and filaments will be necessary to better understand the observed morphology.

3.2.2. *Spectra*

The spectrum of the 3.″7 E position in Figure 4 is similar to previously published spectra (Dinerstein et al. 1987; Ramsay et al. 1993) but has several significant differences. For example, the ratio of Brγ to H_2 $v = 1 \rightarrow 0$ $S(1)$ line emission is ~2 in Ramsay et al.'s spectrum, whereas we find the ratio to be close to 1. A similar discrepancy is seen for the lines of He I at $\lambda = 2.058$ and 2.113 μm. This can perhaps be explained by the different slit sizes used. Ramsay et al. summed spectra over a 3.″1 × 15.″5 region, whereas the spectrum for the 3.″7 E position presented here is summed over a region 1″ × 2.″5. The Ramsay et al. spectrum therefore includes part of the equatorial region edge, and probably a contribution from the core or regions near the core where the H_2 $v = 1 \rightarrow 0$ $S(1)$ line is not detected. There also might be significant scattered emission from the central source at the eastern positions. We also detect about 30 lines in the J and H bands, and the lines seen in the K band by Ramsay et al. plus the following additional lines have been detected: $v = 1 \rightarrow 0$ $S(3)$ (1.9570 μm), 8–6 $O(2)$ (1.9702 μm), 7–5 $O(5)$ (2.0215 μm), 3–2 $S(5)$ (2.0650 μm), 9–7 $Q(2)$ (2.0835 μm), 9–7 $Q(3)$ (2.1001 μm), 3–2 $S(4)$ (2.1274 μm), and 9–7 $O(3)$ (2.2530 μm).

3.3. H_2 *Excitation (Revisited)*

Molecular hydrogen emits a near-IR spectrum through emission from slow electric quadrupole vibration–rotation transitions. There are two mechanisms by which these transitions can be excited. Collisional excitation can occur in gas with kinetic temperatures $T_K \gtrsim 1000$ K (most often associated with moderate velocity shock waves). H_2 can also be excited by absorption of ultraviolet photons with $\lambda > 912$ Å in the Lyman and Werner bands. In low-density regions ($n_{tot} < 10^4$ cm^{-3}) the resulting cascade produces an easily identifiable near-infrared spectrum (Black & van Dishoeck 1987).

Because of its clear spectral signature of UV-pumped H_2, Hb 12 has become the prototype source of near-IR fluorescent H_2 emission. Since regions displaying this type of extreme spectral signature appear to be relatively rare, it is

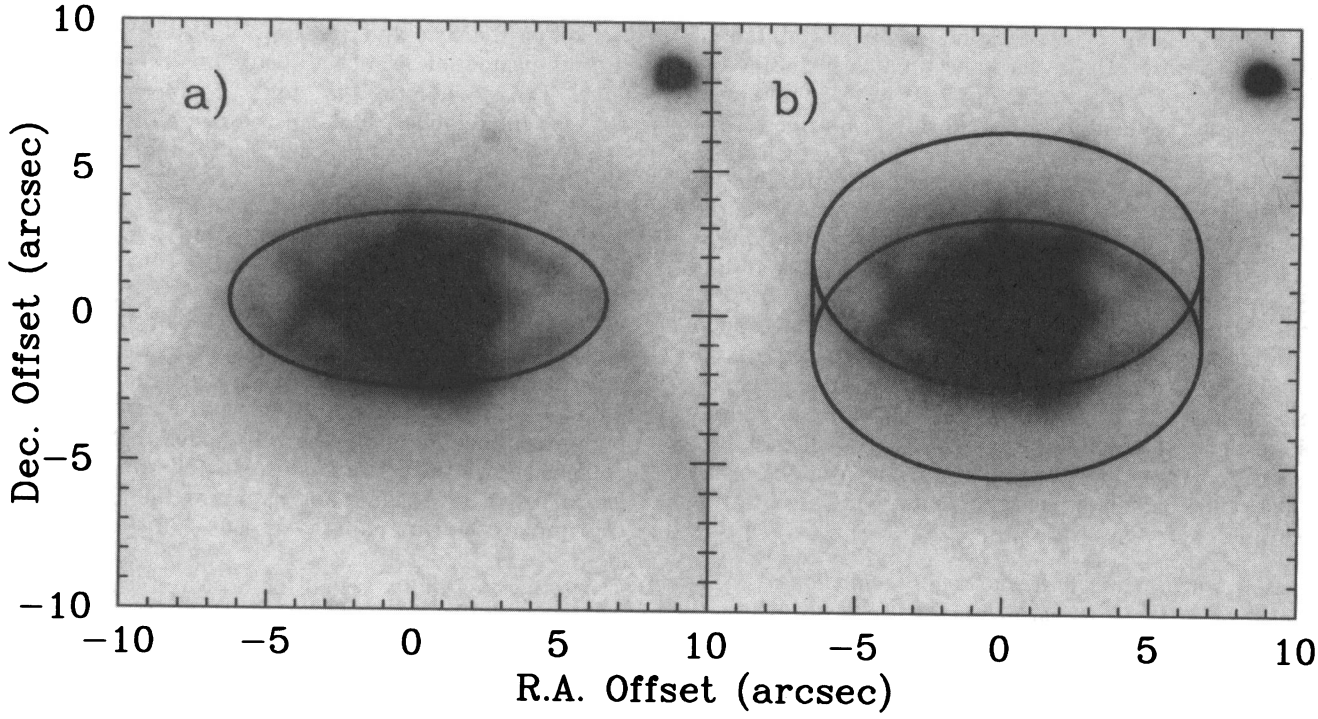

FIG. 6.—Inner 20″ of Hb 12 at 2.12 μm. (*a*) Overlayed with a circle viewed at ~30° from its plane. (*b*) Overlayed with an outline of a short cylinder, its axis tilted ~50° from the plane of the sky.

worthwhile to examine the spectrum of molecular hydrogen from Hb 12 is some detail. Our spectra sensitively cover most of the near-IR J, H, and K bands and give some spatial information. We have, therefore, reexamined the H_2 excitation at two points in the nebula associated with a "knot" of H_2 3".7 E of the core, and a point on the edge of the equatorial region 3".7 E and 2" S of the core. Luhman & Rieke (1996) discuss a long-slit spectrum taken in the east–west direction. Their study provides data that overlaps with ours, provides information on regions in the nebula not previously observed, and goes into greater detail than will be done here.

In the spectrum of the position 3".7 E of the core, ≈ 50 lines of H_2 and ≈ 35 lines in the 3".7 E, 2" S position are detected (Fig. 4 and Table 1). These lines originate from vibrational levels that range from $v = 1$ to $v = 9$. We are, therefore, able to extend the studies of Dinerstein et al. (1988) and Ramsay et al. (1993). The following analysis follows that of Ramsay et al. (1993) for Hb 12, and that of Hora & Latter (1994) as applied to M2–9 and AFGL 2688.

The long spectral baseline of these data allows for a good determination of the differential attenuation in the wavelength region observed. For the spectrum at 3".7 E, we used eight line ratios from 16 different transitions that extend from $\lambda = 1.167$ to 2.423 μm. Six line ratios of the type needed to determine attenuation are available in the 3".7 E, 2" S spectrum. Each ratio was for a line pair originating from the same upper state, making the predicted ratio just the ratio of the products $\Delta E A_{ul}$ for each of the transitions. Several ratios are clearly discrepant, either because of measurement error, or contamination by other emission lines. These ratios were not used in the attenuation determination. Using a standard interstellar extinction law (Rieke & Lebofsky 1985), the visual attenuation toward both positions is estimated to be $A_V \approx 3.7^{+1.5}_{-1.0}$ mag. In all computations presented here, a value of $A_V = 3.5$ mag has been used to deredden the observed H_2 line ratios. In the type of analysis that follows, any errors introduced by departures from a purely interstellar type extinction law, or simply from uncertainty in the value of A_V will be small.

A test of whether the kinetic temperature is high enough to excite the IR emission is the H_2 ortho-to-para ratio. A lower than thermal ratio (the ratio of statistical weights = 3/1) indicates temperatures and densities much lower than are required to collisionally excite the near-IR spectrum. O/P interchange is accomplished through reactions with H^+ and H_3^+ (for example). This is in competition with the H_2 source reaction (grain surface reactions), which is thought to produce H_2 initially in the thermalized 3/1 ratio. Ramsay et al. determined an uncertain ortho-to-para ratio of 1.72 based only on a few lines in the K band. By a similar analysis that used many more line pairs, we find the ortho-to-para ratio to be 1.73 ± 0.2, in excellent agreement with the earlier result. This O/P ratio, therefore, indicates that the H_2 emission is not thermally excited.

In Figure 7 the logarithm of the observed populations (using an ortho-to-para ratio = 1.73) is shown relative to that in the $v = 1$, $J = 3$ level [the origin of the $v = 1 \rightarrow 0$ $S(1)$ line] versus $T_{\rm upper} = E(v', J')/k$. All points would lie on a single straight line if a strict Boltzmann distribution held for the vibration–rotation levels (see, e.g., the case for AFGL 2688 in Hora & Latter 1994). It is clearly evident in Figure 7 that no such straight line exists. However, each set of points from common vibrational levels fall on individual lines for which a single slope applies. The negative inverse of this slope gives the rotational excitation temperature of the molecules along the line of sight. The average rotational excitation temperature found from linear regression to all

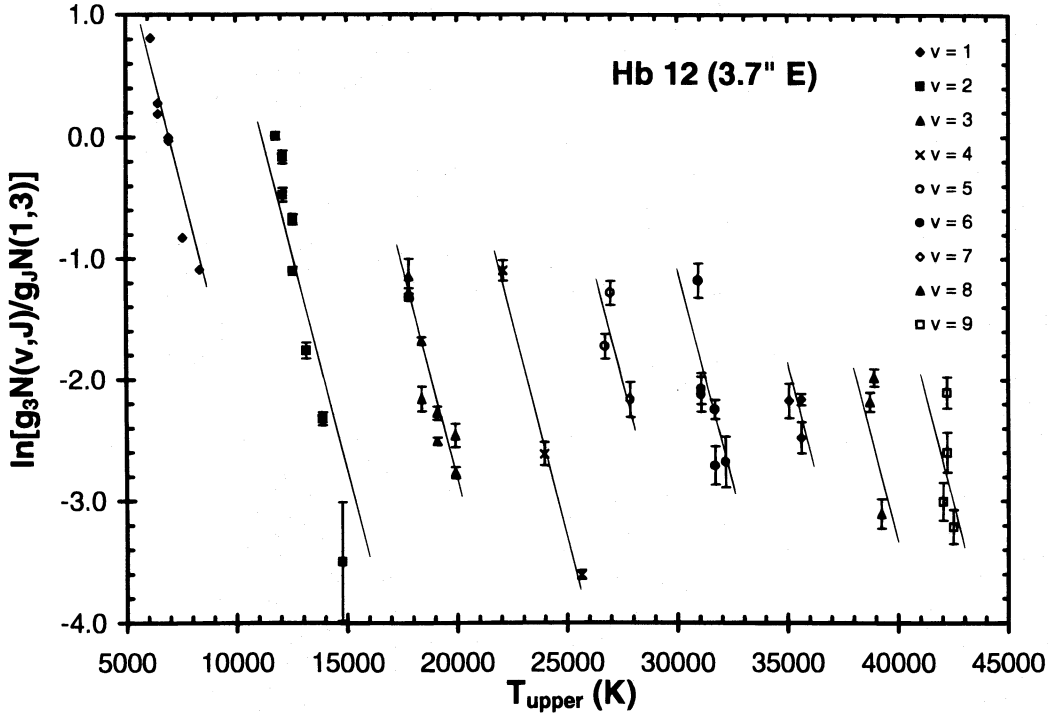

FIG. 7.—Excitation diagram for Hb 12 in the 3".7 E position (dereddened for $A_V = 3.5$ mag). Shown are the upper state vibration-rotation populations relative to that in the $v = 1$, $J = 3$ level vs. the energy of the upper state in Kelvin. Here g_J is the statistical weight, which for odd J levels includes the ortho-to-para ratio of 1.73 (see text). Linear fits to the different vibrational levels finds the rotational excitation temperature to be $T_{\rm ex}(J) = 1395 \pm 450$ K. The lines shown are characteristic for this value of $T_{\rm ex}(J)$. Ratios not used in the analysis because of blending are not plotted.

the points is $T_{ex}(J) = 1395 \pm 450$ K. A vibrational excitation temperature can be determined by comparing lines arising from the same rotational level. We have done this for 27 line pairs and found that no single temperature describes the system. In a general way, the average excitation temperature tends to increase with vibrational level and typically falls in the range $T_{ex}(v) \sim 7000$–13,500 K. These types of excitation temperatures are characteristic of a pure fluorescence spectrum. While the signal-to-noise ratio in the 3".7 E, 2" S spectrum is lower, thereby increasing the uncertainties, the same analysis of that spectrum proves that the 3".7 E, 2" S region has a purely UV excited spectrum as well. We find no clear difference in excitation characteristics for the two locations. If shocks contribute to the excitation of the H_2 within the equatorial region, there is no indication of it in the data presented here.

A comparison of the spectrum at the 3".7 E position with the models of Black & van Dishoeck (1987) was made by directly comparing the observed line ratios with those predicted by their Model 14 ($n_H = 3000$ cm^{-3} and UV field 1000 times the ambient interstellar field). After removal of lines that are known to be contaminated, or are likely to be contaminated by nearby atomic lines, the agreement is excellent. All lines originating from $v = 1$ and $v = 2$ levels typically agree to within 10 to 20%. Discrepancies increase for $v \geq 3$ to a maximum factor of ~ 2.5 for three lines, but all others fall within a factor of 2.0 of the predicted ratios. An even better fit likely could be found by optimizing the density and UV field parameters.

3.4. *A Possible Link between Bipolar Reflection Nebulae and Butterfly Planetary Nebulae*

In many respects, the new H_2 image of Hb 12 in Figure 2 is strikingly similar to that of the more evolved butterfly nebula NGC 2346 (see, e.g., Latter et al. 1995). By comparing these two objects and looking at how Hb 12 compares with younger bipolar nebulae, perhaps some new light can be cast on the evolution of axisymmetric PNs. It is in this area that the distinction of whether or not a thin torus is present can be of some significance.

Hb 12 is clearly in a period of very rapid evolution. Other PNs in a similar state might be NGC 7027 and BD +30°3639. Neither of these objects display fluorescent H_2 emission to the degree found for Hb 12. Given that both have sufficiently strong UV emitting central stars, this likely argues for higher density envelopes, and therefore (perhaps) more massive progenitors with high mass loss rates on the AGB. Those objects, while not spherically symmetric, also do not appear as extremely asymmetric as Hb 12. For these reasons it is difficult, and perhaps not justified to make any direct comparisions with other objects in short periods of rapid evolution.

Even though it is a very young extreme butterfly nebula, Hb 12 has already established features that are directly comparable to more evolved objects like NGC 2346. Also, as a relatively young PN, it might allow us to say something about the morphology of the post-AGB bipolar nebulae. As with Hb 12, the "wings" of NGC 2346 are seen predominantly in H_2 emission. There is also a central elliptical region of filamentary H_2 emission, not unlike that seen in Hb 12. The H_2 emission observed in NGC 2346 is likely from shocked gas at the interface of expanding bubbles (Kastner et al. 1994; Latter et al. 1995), which is unlike Hb 12 where the H_2 emission arises from radiative effects in the photodissociation region (PDR). From the data available so far, we cannot tell what the excitation mechanism is for the H_2 "wings" in Hb 12.

Hb 12 and NGC 2346 likely have evolved from post-AGB objects like AFGL 618 and AFGL 2688. These objects are bipolar reflection nebulae, in which the density of dust decreases with increasing stellar latitude (Morris 1981; Yusef-Zadeh, Morris, & White 1984; Latter et al. 1992, 1993). Molecular hydrogen emission is detected in the lobes of those objects and others like them. AFGL 618 and M2−9 are known to be at a phase in which at least part of the H_2 emission is coming from fluorescent excitation within the PDR (Latter et al. 1992; Hora & Latter 1994). It is possible that we are seeing an evolutionary sequence in these objects—from young to old. It is difficult to know for certain, given the wide range of possible central star and envelope masses. However, the similarities imply a strong relationship. All have a bipolar symmetry and all have H_2 emission arising, at least in part, from the bipolar lobes. These observations are consistent with the lobes being expanding bubbles with the H_2 emission coming from limb-brightened edges.

It has been argued that compact, overdense tori (with a density in excess of what would be deposited by heavy mass loss on the AGB) are not required to explain the observed morphologies of the young bipolar nebulae (see, e.g., Morris 1981; Yusef-Zadeh et al. 1984; Latter et al. 1993). There are exceptions—objects such as AFGL 915 and possibly IRAS 09371+1212 appear to have dense, long-lived disks (Jura, Balm, & Kahane 1995; Roddier et al. 1995). However, for the other objects there is a preferred direction for the mass loss resulting in a lower dust density in the polar regions—it is this lower dust density that produces the observed bipolar shapes in scattered starlight. The central regions of Hb 12 and NGC 2346 are complex, but there is no clear evidence for the remnant of a dense torus of the type required to be the primary mechanism of bipolar shaping. What we find are structures apparently formed by instabilities in interacting winds in axisymmetric distribution of material. This is what would be expected from the above mentioned general morphology of bipolar nebulae, and from a number of recent radiation–gasdynamics models (see, e.g., Mellema 1993; Frank et al. 1993; Frank & Mellema 1994a, b). While large uncertainties remain, Hb 12 might be an important link between the young bipolar nebulae and the evolved butterfly PNs.

4. CONCLUSIONS

Near-IR images and spectra of Hb 12 reveal the complex structure of the inner region of this PN and its large-scale bipolar morphology. UV flux from the bright, unresolved core excites fluorescent emission from H_2 in the equatorial region. The H_2 fluorescence is consistent with low-density ($n < 10^4$ cm^{-3}) gas in this region. The presence of apparently shocked [Fe II] emission in the edge of the equatorial region could signal a transition to higher density material outside of this zone. The images suggest a toroidal or cylindrical structure, which delineates an equatorial density enhancement that is channeling the bipolar flow. The structure compares well with recent radiation-gasdynamic model results that show similar morphologies in early PN development.

We have reexamined the H_2 emission from Hb 12 using new spectral and spatial information. For the 3".7 E posi-

tion, linear fits to the different vibrational levels finds the rotational excitation temperature to be $T_{ex}(J) = 1395 \pm 450$ K, and vibrational excitation temperatures typically fall in the range $T_{ex}(v) \approx 7000$–13,500 K, but no single vibrational temperature describes the excitation. Excellent agreement is seen between the observed line ratios and those predicted by theoretical H_2 fluorescence calculations.

Advances in near-infrared astronomy have helped to provide a good sampling of objects in transition across the top of the HR diagram (Kwok 1996). The goal of providing a clear evolutionary sequence is not yet possible. Any evolutionary sequence of observed objects will be highly uncertain because of extreme differences in evolutionary timescales for objects of differing mass. Continued observations and theoretical modeling are required to establish this connection. However, with Hb 12 now revealed as a possible link between the young bipolar reflection nebulae and the more evolved butterfly PNs, a full description of the evolution of axisymmetric nebulae might be closer at hand.

We wish to express thanks to Lynne Deutsch for her assistance in obtaining the spectral data, and discussion on drafts of the paper. We thank John Black for illuminating conversations and Kevin Luhman for communicating results prior to publication. W. B. L. was supported by the National Research Council.

REFERENCES

Aspin, C., et al. 1993, A&A, 278, 255
Beckwith, S., Persson, S. E., & Gatley, I. 1978, ApJ, 219, L33
Bentley, A. F., Hackwell, J. A., Grasdalen, G. L., & Gehrz, R. D. 1984, ApJ, 278, 665
Bignell, R. C. 1983, in IAU Symp. 103, Planetary Nebulae, ed. D. R. Flower (Dordrecht: Reidel), 69
Black, J. H., & van Dishoeck, E. F. 1987, ApJ, 322, 412
Dinerstein, H. L., Lester, D. F., Carr, J. S., & Harvey, P. M. 1988, ApJ, 327, L27
Elias, J. H., Frogel, J. A., Mathews, K., & Neugebauer, G. 1982, AJ, 87, 1029
Frank, A., Balick, B., Icke, V., & Mellema, G. 1993, ApJ, 404, L25
Frank, A., & Mellema, G. 1994a, ApJ, 430, 800
———. 1994b, A&A, 289, 937
Graham, J. R., Serabyn, E., Herbst, T. M., Matthews, K., Neugebauer, G., Soifer, B. T., Wilson, T. D., & Beckwith, S. 1993, AJ, 105, 250
Hodapp, K. W., Hora, J. L., Irwin, E., & Young, T. 1994, PASP, 106, 87
Hora, J. L., & Latter, W. B. 1994, ApJ, 437, 281
Johnson, H. M., Balick, B., & Thompson, A. R. 1979, ApJ, 233, 919
Jura, M., Balm, S. P., & Kahane, C. 1995, ApJ, 453, 721
Kastner, J. H., Gatley, I., Merrill, K. M., Probst, R., & Weintraub, D. A. 1994, ApJ, 421, 600
Kelly, D. M., & Latter, W. B. 1995, AJ, 109, 1320
Kohoutek, L., & Martin, W. 1981, A&A, 94, 365
Kozlowski, L. J., et al. 1994, in Proc. SPIE 2268, Infrared Spaceborne Remote Sensing, 353
Kwok, S. 1996, in IAU Symp. 170, CO: Twenty-five Years of Millimeter-wave Spectroscopy, ed. W. B. Latter, J. Bally, P. R. Jewell, J. G. Mangum, & S. Radford (Dordrecht: Kluwer), in press
Latter, W. B., Hora, J. L., Kelly, D. M., Deutsch, L. K., & Maloney, P. R. 1993, AJ, 106, 260
Latter, W. B., Kelly, D. M., Hora, J. L., & Deutsch, L. K. 1995, ApJS, 100, 159
Latter, W. B., Maloney, P. R., Kelly, D. M., Black, J. H., Rieke, G. H., & Rieke, M. J. 1992, ApJ, 389, 347
Linde, P., & Johannesson, A. 1991, in 3d ESO/ST-ECF Data Analysis Workshop, ed. P. J. Grosbol & R. H. Warmels (Garching: ESO), 173
Luhman, K., & Rieke, G. H. 1996, ApJ, 461, in press
Mellema, G. 1993, Ph.D. thesis, Sterrewacht Leiden
Miranda, L. F., & Solf, J. 1989, A&A, 214, 353
Morris, M. 1981, ApJ, 249, 572
Ramsay, S. K., Chrysostomou, A., Geballe, T. R., Brand, P. W. J. L., & Mountain, M. 1993, MNRAS, 263, 695
Rieke, G. H., & Lebofsky, M. J. 1985, ApJ, 288, 618
Roddier, F., Roddier, C., Graves, J. E., & Northcott, M. J. 1995, ApJ, 443, 249
Rudy, R. J., Rossano, G. S., Erwin, P., Puetter, R. C., & Feibelman, W. A. 1993, AJ, 105, 1002
Scott, P. F. 1973, MNRAS, 161, 35
Sternberg, A., & Dalgarno, A. 1989, ApJ, 338, 197
Storey, J. W. V. 1984, MNRAS, 206, 521
Yusef-Zadeh, F., Morris, M., & White, R. L. 1984, ApJ, 278, 186